Computational Study on Purification of CO_2 from Natural Gas by C_{60} Intercalated Graphite

Xuan Peng,*,† Dapeng Cao,‡ and Wenchuan Wang‡

College of Information Science and Technology, Beijing University of Chemical Technology, Beijing 100029, Guangzhou Center for Gas Hydrate Research, Chinese Academy of Sciences, Guangzhou 510640, P. R. China, and Division of Molecular and Materials Simulation, Key Lab of Nanomaterials, Ministry of Education, Beijing University of Chemical Technology, Beijing 100029, P. R. China

By combining grand canonical Monte Carlo (GCMC) simulations with adsorption theory, we perform a computational study on adsorption of CH_4 and CO_2 gases and purification of CO_2 from the CH_4-CO_2 and N_2-CO_2 binary mixtures by the C_{60} intercalated graphite. The adsorption isotherms, isosteric heats and snapshots of pure gases have been examined extensively. It is found that the maximum excess uptakes at 298 K are relatively low, only giving 4.04 and 4.96 mmol/g for CH_4 and CO_2, respectively, due to a low porosity of 0.45 and a large crystal density of 1.57 g/cm^3 of this material. It indicates that the pristine material is not suitable for gas storage. However, this material provides excellent selectivity for CO_2, and the selectivity at ambient condition can reach 8 and 50 for the CH_4-CO_2 and N_2-CO_2 mixture, respectively. Furthermore, the selectivity of CO_2 is almost independent of the bulk gas composition for $P > 0.1$ MPa. The dual-site Langmuir−Freundlich (DSLF) equation is used to fit the adsorption isotherms of pure gases from GCMC simulations, and the corresponding parameters are obtained. Moreover, we further predicted the adsorption behavior of binary mixtures by the DSLF-based ideal adsorption solution theory (IAST). Although the IAST theory slightly overestimates the selectivity, compared to GCMC results, the uptakes and selectivity from both methods are basically consistent. To improve the adsorption capacities, we further tailor the structural parameter "g" of the C_{60} intercalated graphite by GCMC simulations. For equimolar gas composition, at the condition of $g = 1.4$ nm and 6 MPa, the CO_2 uptakes could be raised by 200%, approaching 12 mmol/g for both mixtures, without loss of the selectivity for CO_2. In summary, this work demonstrates that the C_{60} intercalated graphite is an excellent material for CO_2 purification, especially for N_2-CO_2 system at room temperature.

Introduction

Porous carbon materials are extensively applied in gas storage[1,2] and separation[3,4] for their hydrothermal and chemical stabilities. Graphite nanofibers (GNFs) that consist of parallel graphitic platelets stacked in layers forming fibers many micrometers in length, is a typical representative of porous carbons.[5] Rodriguez and co-workers have proposed that the GNFs is a promising adsorbent for H_2 storage because the experiment shows that the material can adsorb a great deal of H_2 at room temperature.[6,7] However, this viewpoint has been subsequently questioned by the grand canonical Monte Carlo (GCMC) simulation studies from Wang and Johnson.[5,8] They concluded that the experimental results could not be interpreted by any reasonable physisorption model. Recent studies have shown that the interlayer distance of the GNFs is the key to determine the H_2 uptake.[9−11] In a slit pore model, the optimum pore size for the maximum storage capacity was around 0.6 nm.[9−11] At the interlayer distance of 0.335 nm, the H_2−graphene interaction is repulsive and thus no H_2 can penetrate between the graphite layers. But if the graphene sheets are intercalated by spacer molecules, the interlayer distance could be increased to meet the requirement of the optimum pore size.

C_{60} fullerenes[12,13] are suitable spacer molecules intercalated to graphite. Actually, using C_{60} as intercalation reagent initially originated from the development of a new class of superconductors.[14] In 1994, Saito et al. first designed the model of C_{60} intercalated graphite and theoretically predicted the stability of such structures.[14] Until 2004, Gupta and co-workers synthesized for the first time this carbon material by directly combining two carbon allotropes of C_{60} and graphite.[15] During the intercalation process, the van der Waals (vdW) contact between two adjacent parallel layers is broken and a two-dimensional hexagonal symmetry of C_{60} fullerenes is formed. The transmission electron microscopy (TEM) image indicates that no covalent bonds exist between fullerenes, and between the fullerenes and the layers. Recently, using density functional theory (DFT) calculation, Kuc et al. confirmed the experimentally observed geometrical properties of the C_{60} intercalated graphite and evaluated its capability for H_2 storage.[16] Their study indicates that this material may be promising to store H_2.

Besides H_2 storage, carbon dioxide capture and storage (CCS) has become one of the most urgent topics worldwide.[17] The exhausted exploitation of fossil fuels in industrial processes increases the concentration of CO_2 in the atmosphere and leads to the serious problem of global warming.[18] For example, the methane steam reforming reaction, which uses CH_4 and water vapor as raw materials to produce H_2, is a major industrial source of CO_2 as a byproduct. Additionally, CH_4 and CO_2 are the primary components in natural gas, except for N_2 and heavier hydrocarbons.[3] The existence of CO_2 will reduce the energy content of natural gas and corrupt the transportation and storage system.[3] As a consequence, CH_4 storage and CO_2 removal are equally important to effectively utilize the energy and sequestrate the greenhouse gases.

* To whom correspondence should be addressed. Tel.: +86 010 64443254. E-mail: pengxuan@mail.buct.edu.cn.

† College of Information Science and Technology, Beijing University of Chemical Technology and Chinese Academy of Sciences.

‡ Ministry of Education, Beijing University of Chemical Technology.

10.1021/ie1010433
Published on Web 08/05/2010

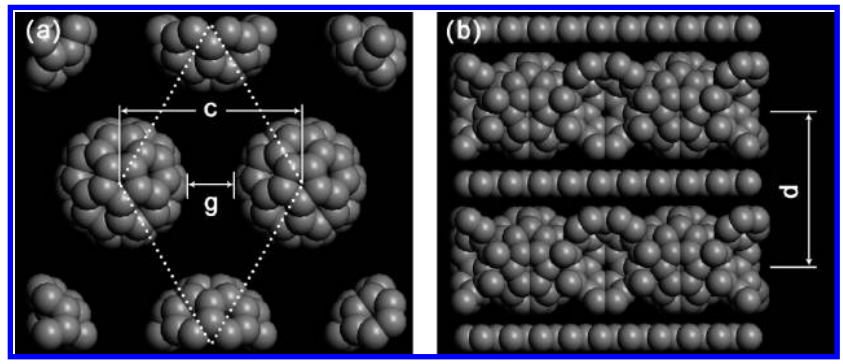

Figure 1. Structure of C_{60} intercalated graphite: (a) top view, where graphite layers are hidden for clarity; (b) side view.

To the best of our knowledge, no experimental and theoretical studies have been conducted on the adsorption storage of CH_4 and purification of CO_2 by using the C_{60} intercalated graphite. In 2009, Terzyk et al. investigated the storage of these gases on intercalated graphene nanocontainers (NanoBuds) by using GCMC simulations.[19] They found that intercalation can improve the storage, in which the fullerenes of C_{180} other than C_{60} were used as intercalation reagent to construct the model of material. The adsorption behavior of gases on pristine C_{60} intercalated graphite is still unknown. Furthermore, the selectivity of this material for CO_2 is not reported yet. Accordingly, here we intend to explore the adsorption and selectivity of this material for CO_2 by using a computational method. This paper is organized as below. First, we describe the structural and potential models, and the detail of molecular simulation and adsorption theory. Then, we perform the studies of adsorption storage and separation of the C_{60} intercalated graphite for CO_2. Finally, we also further tailor the structural parameters to improve the adsorption and separation properties of this material.

Molecular Simulation

Structure of C_{60} Intercalated Graphite. As shown in Figure 1, the hexagonal area surrounded by dotted lines constitutes a lattice. The variables c and d denote the lattice constant and the distance between the centers of C_{60} on two adjacent planes, and their values are 1.25 and 1.27 nm, taken from experimental measurement, respectively. The variable g is defined as the distance between the centers of outmost carbon layer on two adjacent C_{60} fullerenes and equals to c minus the diameter of C_{60}. In molecular simulations, the structure of the material is assumed to be rigid without geometrical variation. To create the structure of the C_{60} intercalated graphite, we used one C_{60} molecule and one graphite plane with a chirality of (13,0) and a length of 3.2 nm as the elements. Then, we reproduced the C_{60} molecule 15 times and the graphite plane 2 times and translated them to the suitable positions in terms of the structural schematic given by Kuc et al.[16] Finally, we cut the structure to generate a rectangular simulation unit cell. Thus, for the default structure without refinement, there are 1080 carbon atoms in the unit cell and the cell size is 2.5, 2.165, and 2.54 nm in the x, y, and z dimensions, respectively.

Potential Models. As usual, N_2 and CH_4 molecules are regarded as a single sphere, and the classical Lennard-Jones (LJ) potential is used to calculate their interactions.[1,2,20,21] As for the CO_2 molecule with a linear geometry and noticeable quadrupole moment, the 3-site elementary physical model (EPM2) was used, where a three-center LJ potential plus a set of partial point charges is distributed at three electrostatic sites.[22,23] Thus, the fluid−fluid interaction of CO_2 is composed of the LJ potential and electrostatic interactions. The fluid−solid interaction is described by the site-to-site method and the cross interaction parameters are obtained by the Lorentz−Berthelot combining rules. All the size and energy parameters of fluid molecules and adsorbent were given in Table 1.

Table 1. Potential Parameters of N_2, CH_4, CO_2, and C_{60} Intercalated Graphite

species	atom	bl (nm)[a]	q (e)	σ (nm)	ε/k_b (K)	ref
N_2				0.375	95.2	2, 20
CH_4				0.381	148.2	1, 21
CO_2	C	0.0	0.6512	0.2757	28.129	22, 23
	O	0.1149	−0.3256	0.3033	80.507	
adsorbent	C			0.34	28.0	1, 2

[a] bl is the distance from the interaction site to molecular mass center.

Simulation Details. We used the GCMC method[24,25] to study the adsorption and separation of gases in the C_{60} intercalated graphite. In this method, the chemical potential, box volume and temperature are fixed in the simulation. For N_2 and CH_4 molecules, the GCMC procedure includes particle translation with the usual Metropolis scheme, particle destruction, and creation to ensure the chemical potential equilibrium between bulk and pore phases, while for the CO_2 molecule, an additional move of particle rotation is needed. For the adsorbent structure model used here, the inner void space of C_{60} intercalated graphite is not blocked and thus GCMC simulations can insert molecules directly into these voids. Although it is theoretically possible, the probability of inserting such molecules is extremely low. To avoid the conversion of chemical potential into pressure, the normal move acceptance probability can be transformed to relate the component fugacity of the bulk phase, which is calculated by the Peng−Robinson equation of state (PR EOS).[26] The binary interaction parameters in the PR EOS are +0.092 and −0.017 for the CH_4−CO_2 and N_2−CO_2 mixture, respectively.[27] For all the simulations, the periodic boundary conditions were imposed in three directions. The cutoff radius is set to half the box size for the LJ and electrostatic potentials. On the basis of the simulation cell dimensions of the pristine structure, the cutoff distance for LJ and electrostatic potentials is 1.0825 nm. For the LJ potential, the cutoff is usually adequate. However, for the electrostatic potential, since we did not use the Ewald sum to save computational time, justification for the cutoff needs to compare the results with that from a larger simulation cell. In our test run, we used the C_{60} intercalated graphite with the doubled cell dimensions for comparison. We found that both results are basically consistent and the average deviation is no more than 3%. To accelerate the simulation, the LJ potential between a fluid molecule and adsorbent was substituted by a pretabulated energy map with a grid of $0.2 \times 0.2 \times 0.2$ Å cubic mesh. For each state, a total number of 2×10^7 configurations were generated, where the first 40% moves

were discarded to guarantee the equilibrium and the others were divided into 20 blocks for the ensemble average. All the simulations here were performed using the MUSIC code.[28]

Definitions of Adsorption Amount, Isosteric Heat, and Selectivity. The excess adsorption amount N_{ex}, which can be measured experimentally, is commonly calculated by the absolute adsorption amount N_{ab} from GCMC simulation according to the following relation

$$N_{ex} = N_{ab} - \rho_b V_{av} \quad (1)$$

where ρ_b is the bulk density obtained by PR EOS and V_{av} is the available volume to fluid molecules. Different from the other method integrating the configurational energy of the adsorbed molecule, we performed a Monte Carlo integration with the reentrant surface definition[29] to calculate the V_{av}, where the argon molecule with a size of 0.34 nm was used as a probe.[30] The porosity is expressed by the ratio of V_{av} to the adsorbent volume. The method had been tested for the porosity of the IRMOF-1 material, and it gives excellent agreement with the value reported.[31]

The isosteric heat q_{st}, a thermodynamic property that reflects the strength of forces between adsorbent and fluid molecules, is approximated by[31]

$$q_{st} \approx RT - \left(\frac{\partial U}{\partial N}\right)_{T,V} \quad (2)$$

where R and T are the universal gas constant and temperature and U and N are the total adsorbed energy and number of fluid particles, respectively.

The adsorption selectivity of CO_2 in N_2-CO_2 and CH_4-CO_2 binary mixtures is defined as

$$S_{i/j} = \left(\frac{x_i}{y_i}\right)\left(\frac{y_j}{x_j}\right) \quad (3)$$

where subscript i denotes CO_2, subscript j denotes the species N_2 or CH_4, and x and y denote the molar fractions of species in adsorbed and bulk phases, respectively.

Adsorption Theory

Fitting of Pure Adsorption Isotherms from GCMC Simulations. As is well-known, no experimental data are available for adsorption of the pure and binary mixtures of the $N_2-CH_4-CO_2$ system in the C_{60} intercalated graphite. To examine the results from molecular simulation, the dual-site Langmuir−Freundlich (DSLF) adsorption model is adopted.[31] Therefore, the pure-component equilibrium data were used to correlate theoretical models, and to further predict the adsorption of mixtures, aiming at the comparison with those from molecular simulation. The DSLF model is given by

$$N^{\circ}(f) = \frac{N_1 k_1 f^{n_1}}{1 + k_1 f^{n_1}} + \frac{N_2 k_2 f^{n_2}}{1 + k_2 f^{n_2}} \quad (4)$$

where f is the fugacity of the bulk gas at equilibrium with the adsorbed phase and in the units of MPa here and N_i, k_i, and n_i are model parameters of maximum adsorption amount at site i ($i = 1$ or 2), the affinity constant, and the deviation from the simple Langmuir equation, respectively.

Prediction of Binary Mixture Adsorption by IAST Theory. On the basis of the available model parameters of pure gas adsorption, we used the ideal adsorption solution theory (IAST),[32] which proposed by Myer and Prausnitz in 1965, to predict the multicomponent adsorption. Analogous to Raoult's law for vapor−liquid equilibrium, the IAST assumes that the adsorbed solutions are ideal and all activity coefficients in the adsorbed phase are unity. Thus, the adsorption equilibrium between adsorbed and gas phases will lead to the following equation

$$P y_i \phi_i = x_i f_i^{\circ}(\pi) \quad (5)$$

where f_i° is the fugacity of the equilibrium gas phase corresponding to the spreading pressure π for the adsorption of pure gas i, ϕ_i is the gas fugacity coefficient of component i calculated by PR EOS, and x_i and y_i are the molar fraction of component i at adsorbed and bulk phases, respectively. The binary gas mixing process is carried out at constant spreading pressure π and indicated by

$$\int_0^{f_1^{\circ}} N_1^{\circ}(f_1) \mathrm{d} \ln f_1 = \int_0^{f_2^{\circ}} N_2^{\circ}(f_2) d \ln f_2 \quad (6)$$

where the single-component adsorption amount and selectivity are further obtained from the above equation by numerical integration and root exploration.

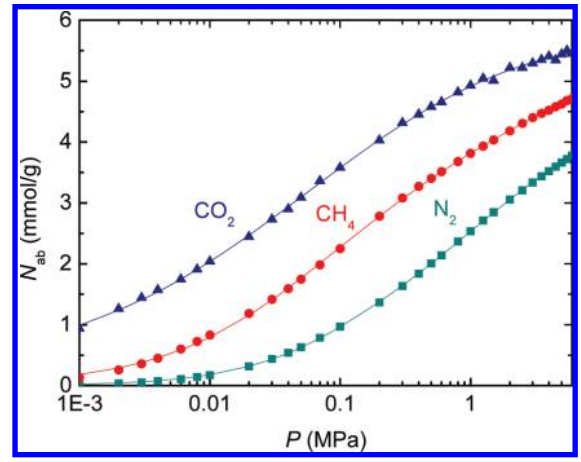

Figure 2. Absolute adsorption isotherms of pure gases in C_{60} intercalated graphite at 298 K. The filled symbols are GCMC simulation results, and the lines are fits of the dual-site Langmuir−Freundlich equation to GCMC simulation results.

Results and Discussion

Adsorption for Pure N_2, CH_4, and CO_2 on C_{60} Intercalated Graphite. Figure 2 shows the absolute adsorption isotherms of pure gases on the C_{60} intercalated graphite at 298 K. As expected, the adsorption amount increases with pressure. At the same pressure, the uptake of CO_2 is the largest, and that of N_2 is the smallest. At $P = 6$ MPa, the uptakes of CH_4 and CO_2 are 4.71 and 5.46 mmol/g, respectively. It is comparable to the experimental results of 4.83 and 7.99 mmol/g in dry activated carbon at 318.2 K and similar pressures.[33] In addition, the adsorption amounts are much less than IRMOF-1 adsorbent with very high values of 17.0 and 28.0 mmol/g for both gases at the same conditions.[31] There are two main reasons responsible for the large difference. On one hand, the C_{60} intercalated graphite owns a smaller porosity of 0.45, which approximates to half of the IRMOF-1 material (0.82). Since a large pore volume is advantageous to the storage capacity at high pressures, a greater uptake should be expected in the IRMOF-1 case. Actually, no particles can be adsorbed on top and bottom positions of the C_{60} fullerenes (see top view in Figure 3) because the space between the graphite and C_{60} fullerene is too narrow

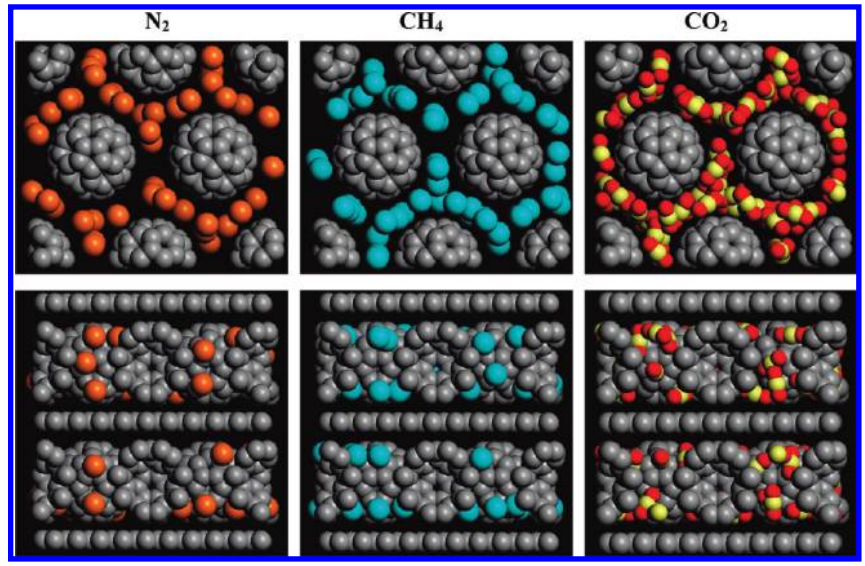

Figure 3. Snapshots of pure gas adsorption in C_{60} intercalated graphite at 298 K and 6 MPa: top, top view; bottom, side view.

to accommodate any fluid molecule. As a result, the adsorption only occurs in the space between the two adjacent C_{60} fullerenes. At the distance g of 0.55 nm, the fluid molecules are adsorbed in a single layer by confinement and form a ringlike structure where two rings are interconnected side by side (top view). Even at this low porosity, the pore volume is not filled completely by adsorbed molecules (side view). On the other hand, the crystal density of the C_{60} intercalated graphite is estimated to be 1.57 g/cm^3, about 2.65 times that of IRMOF-1 adsorbent.[31] Since the gravimetric loading is inversely proportional with the bulk density of material, the large crystal density would lead to the decrease of the adsorption.

The excess adsorption isotherms of pure gases are plotted in Figure 4. Due to the faraway supercritical state at 298 K, we do not find the maximum on the N_2 adsorption isotherm. Instead, a maximum of excess uptake is noticeably observed at 3.5 and 2 MPa for CH_4 and CO_2, respectively. In addition, both the gravimetric and volumetric uptakes are relatively low at the whole pressure range, less than 4.035 mmol/g and 141.6 v/v for CH_4, and 4.959 mmol/g and 174.04 v/v for CO_2. In particular, the volumetric adsorption of CH_4 is lower than the DOE target of 180 v/v at 3.5 MPa and 298 K that proposed by the U.S. Department of Energy.[34] It reveals that the C_{60} intercalated graphite with the pristine structure cannot meet the requirement of gas storage at ambient temperature.

The adsorption isotherm at low pressures usually reflects essential characteristic of material. Thus, we calculate the Henry constant of each species by using the adsorption data at 0.001 MPa. They are 0.019, 0.135, and 0.939 mmol/kPa for N_2, CH_4, and CO_2, respectively, in which CO_2 shows the greatest value of about 49 times of N_2 and 7 times of CH_4. It indicates that the CO_2 molecule has a stronger fluid−pore interaction than other species. For a further explanation, we present in Figure 5 the isosteric heat q_{st} as a function of absolute adsorption amount. We can see that the q_{st} first gradually increases with the uptake to a faint maximum for N_2 (22.58 kJ/mol) and CH_4 (28.44 kJ/mol) at about 0.5 mmol/g, and finally falls down slightly. As to CO_2, the q_{st} drops from 39.06 kJ/mol all along until 4.5 mmol/g, and then fluctuates with the uptake owing to the near-condensation state of bulk phase. Moreover, the varied range of q_{st} approaches that of the C_{168} material for CH_4 and CO_2 but is significantly greater than IRMOF-1 adsorbent.[28] Similarly, the q_{st} presents an increase with the same species order as found in Figure 2 for the adsorption isotherms. This phenomenon also confirms the above conclusion from the Henry constant; i.e., the CO_2 molecule is preferentially adsorbed.

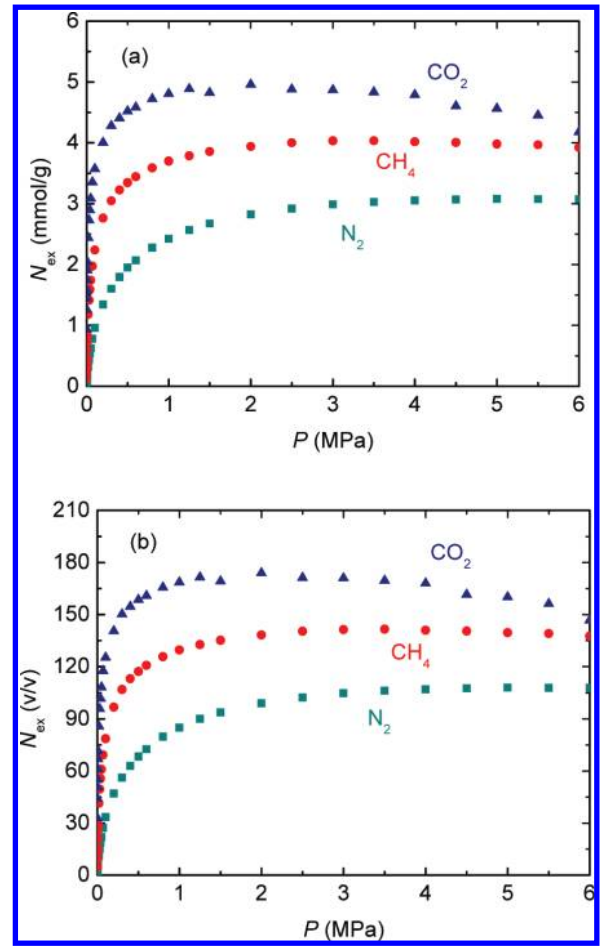

Figure 4. Excess adsorption isotherms of pure gases in C_{60} intercalated graphite at 298 K: (a) in units of mmol/g; (b) in units of v/v.

Purification of CO_2 from N_2−CO_2 and CH_4−CO_2 Binary Mixture on C_{60} Intercalated Graphite. As discussed above, the gas storage performance of the C_{60} intercalated graphite is not satisfactory. However, by comparison with Henry's constant, it is found that this material might be

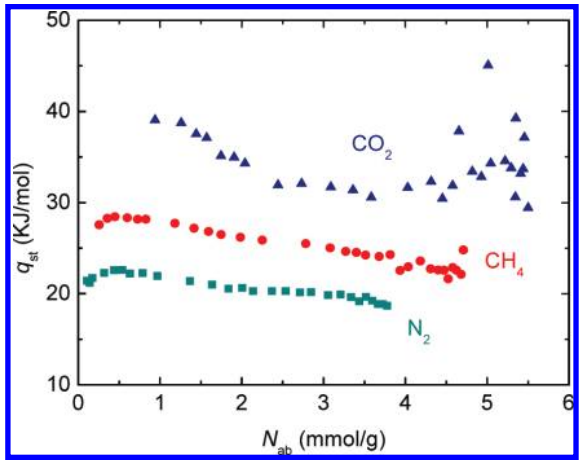

Figure 5. Isosteric heat versus absolute adsorption amount of pure gases in C_{60} intercalated graphite at 298 K.

promising for CO_2 purification from mixtures, because the Henry constant of CO_2 is obviously much greater thanthat of the other two gases. Therefore, we study the adsorption separation of CO_2 in the C_{60} intercalated graphite. The adsorption behavior of CO_2 in gas mixtures could be predicted by GCMC simulation and validated by adsorption theory like the IAST. It is acknowledged that at high pressures the IAST will produce a big deviation from experiment due to the fluid nonideality. To examine this point, we test the approach by using the experimental data reported on activated carbon.[31] From Figure 6, we can see that even at a high pressure up to 13 MPa, both the fitting and the IAST prediction are in excellent agreement with experiment. It demonstrates that if a suitable adsorption model is adopted for pure gases, the IAST approach used here is still effective for the prediction of binary mixtures.

Figure 2 shows the fitting of the DSLF equation to GCMC simulation results for the C_{60} intercalated graphite. To further explore the fitting effect, the average relative deviation (ARD) from GCMC simulation is given in Table 2, in which CO_2 gives the best fitting with the smallest ARD of 0.75%, CH_4 with ARD of 2.5%, and N_2 with ARD of 3.35%. On the whole, the fitting is quite good in view of the large number (31) of data points evaluated. Using the regressed model parameters in Table 2, we investigate the separation performance of CO_2 in the C_{60} intercalated graphite by IAST prediction. In general, an equimolar composition is a good choice for a binary mixture. A mole fraction of $y_{CO_2} = 0.2$ is also specified for the CH_4-CO_2 and N_2-CO_2 mixtures, because the former represents a rich CH_4 natural gas, while the latter represents the postcombustion mixtures. Figure 7 shows the comparison of the single-component adsorption isotherms between the IAST prediction and GCMC simulation. It is found that all the GCMC simulation data are very consistent with the IAST prediction curves. For both mixtures, the uptake of CO_2 at $y_{CO_2} = 0.5$ is always higher than that at $y_{CO_2} = 0.2$, indicating that C_{60} intercalated graphite prefers the CO_2 in a rich CO_2 gas mixtures. Interestingly, the uptake of N_2 is almost close to zero for both gas compositions. Clearly, this material exhibits an excellent selectivity of CO_2 for the N_2-CO_2 mixture.

Figure 8 shows the adsorption selectivity of CO_2 in the C_{60} intercalated graphite at 298 K, in which the IAST predictions overestimate the selectivity slightly, compared to the GCMC simulation results. This phenomenon can be explained by the ARD of fractional uptakes between both methods (see Table 3). The ARD of CO_2 is distinctly lower than other species, varying in the range 1.5−5%. In contrast, N_2 and CH_4 process

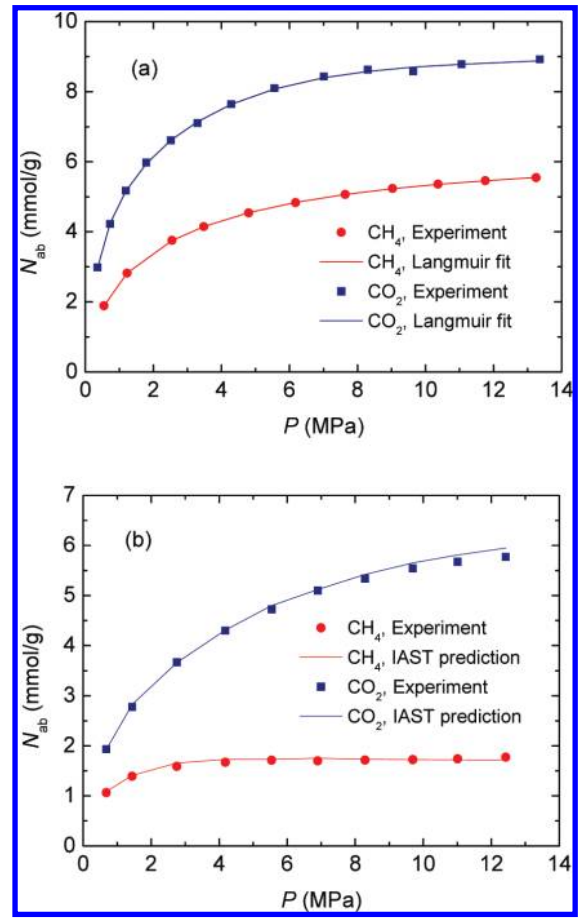

Figure 6. Comparison of the calculated adsorption amount of a single component of CH_4-CO_2 mixture with experimental data on dry activated carbon at 318.2 K in the literature:[33] (a) pure gases; (b) CH_4-CO_2 mixture with CH_4 feed composition of 40.1%.

Table 2. Parameters of Dual-Site Langmuir−Freundlich Equation by Fitting Absolute Adsorption Isotherms from GCMC Simulations

fluid	N_1	k_1	n_1	N_2	k_2	n_2	ARD (%)[a]
N_2	2.9721	0.6042	0.8679	1.6159	6.9512	0.9199	3.35
CH_4	3.7205	6.8673	0.7140	2.1093	0.3785	0.6857	2.50
CO_2	2.3036	3.3656	0.3215	3.9159	4.2120	0.5341	0.75

[a] ARD is the average relative deviation of fitted results from GCMC simulations, and 31 data points were evaluated for each isotherm.

much larger ARD of about 20% and 8%, respectively. In a competitive adsorption with CO_2, these two gases, especially N_2, are rarely adsorbed in the C_{60} intercalated graphite. As a consequence, a slight change of their uptake would result in a remarkable fluctuation of selectivity. This point has also been verified in Figure 8 by a visible deviation of selectivity between both methods. More interestingly, a maximum on the IAST prediction curve of $y_{CO_2} = 0.2$ appears, whereas no maximum is found for the GCMC simulations. Although the reason for this difference is unknown, the variation trend of selectivity curves from both methods is totally coincident and the agreement is acceptable. For the CH_4-CO_2 mixture, the selectivity of CO_2 goes down from about 14 to 8 and then begins leveling off at 100 kPa. The N_2-CO_2 mixture shows a similar trend but the selectivity drops from 120 to 50. In addition, the bulk composition has no pronounced effect on selectivity. At $P <$ 0.1 MPa, the C_{60} intercalated graphite is favorable for separation of CO_2 from a rich CO_2 mixture ($y_{CO_2} = 0.5$), but this favorite gradually becomes negligible when $P > 0.2$ MPa. Figure 9 presents the snapshots of a binary mixture at equimolar

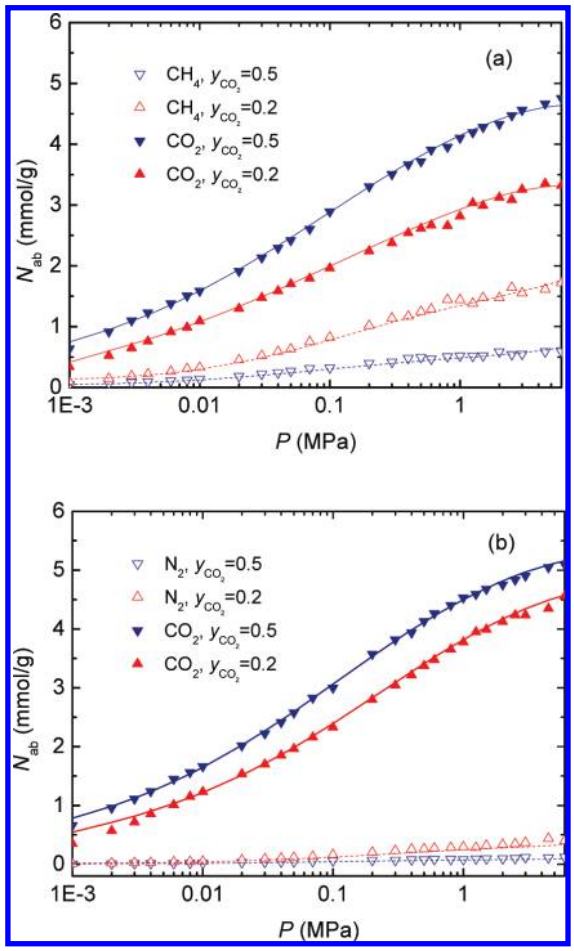

Figure 7. Absolute adsorption isotherms of binary mixtures in C_{60} intercalated graphite at 298 K: (a) CH_4-CO_2 mixture; (b) N_2-CO_2 mixture. The filled symbols are GCMC simulation results, and the lines are IAST predictions.

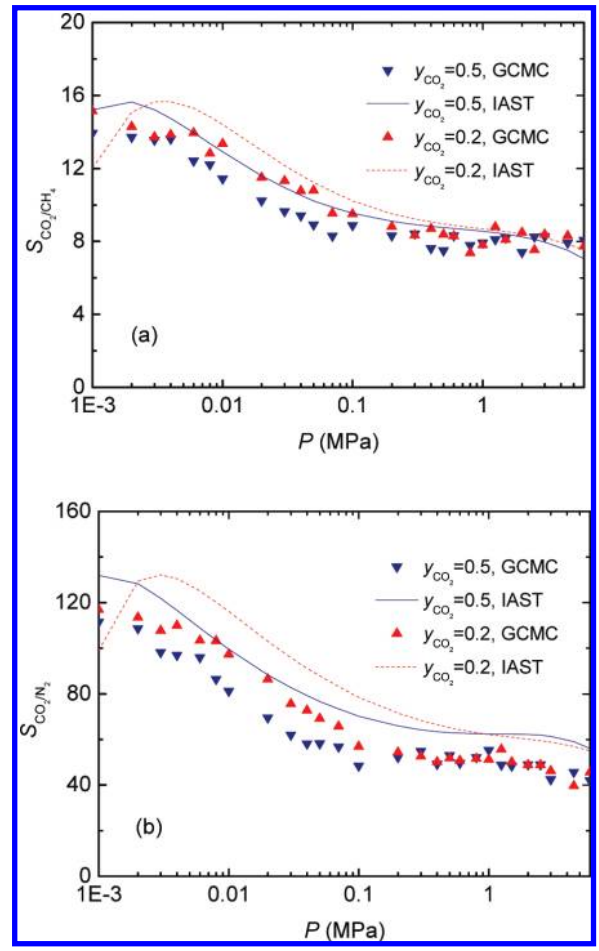

Figure 8. Adsorption selectivity of CO_2 in C_{60} intercalated graphite at 298 K: (a) CH_4-CO_2 mixture; (b) N_2-CO_2 mixture. The filled symbols are GCMC simulation results, and the lines are IAST predictions.

composition. For the N_2-CO_2 mixture, the material is fully filled with CO_2 molecules at three pressure points. Likewise, there are only several CH_4 molecules observed for the CH_4-CO_2 mixture at 0.1 and 6 MPa. For comparison, the theoretical studies on other model carbon materials, such as slit pores,[35] carbon nanotubes,[36] and C_{168} schwarzite[37] are discussed here. For slit pores, at $y_{CO_2} = 0.5$, 318 K and 10 MPa, the selectivity of CO_2 over CH_4 is about 5.6 at the reduced pore width of $H^* = 3$ (1.13 nm),[35] while it is 11.1 for nanotubes with a pore diameter of 1.356 nm at 303 K and 1 MPa and 5.4 for C_{168} schwarzite at 298 K and 0.1 MPa, respectively. It is clear that the C_{60} intercalated graphite shows a superior performance than C_{168} schwarzite and slit pores and nearly approaches nanotubes. As to the N_2-CO_2 mixture, Jiang and Sandler[37] illustrated that in the C_{168} schwarzite the ab initio potential-based GCMC simulation result of selectivity of CO_2 over N_2 at $y_{CO_2} = 0.21$ and 300 K is significantly larger than the Steele potential-based one.[38,39] At 0.1 MPa, the Steele potential-based selectivity of CO_2 over N_2 is about 20, only being one-third of the C_{60} intercalated graphite at the similar condition. Although their result with the ab initio potential can be increased to 100 for the C_{168} schwarzite, the identical ascending behavior should be expected in the C_{60} intercalated graphite if an ab initio potential is used by accounting for the effects of the surface curvature on the C_{60} fullerenes. In summary, we propose that the C_{60} intercalated graphite is an excellent candidate for CO_2 purification at normal temperature and pressure, especially for the N_2-CO_2 system.

Table 3. Average Relative Deviation of Single-Component Adsorption Amounts between IAST Prediction and GCMC Simulations

	ARD (%)[a]			
y_{CO_2}	CH_4	CO_2	N_2	CO_2
0.5	8.358	1.957	19.76	1.756
0.2	7.485	3.632	20.53	4.880

[a] ARD is the average relative deviation of IAST predictions from GCMC simulations, and 27 data points were evaluated for each isotherm.

Structural Refinement of C_{60} Intercalated Graphite for Storage of Pure CH_4 and CO_2, as Well as Purification of CO_2. On the basis of the above information, we conclude that the primary obstacle to the applications of the C_{60} intercalated graphite into gas storage and purification is the low adsorption capacity with the pristine structure. Therefore, in this section, we discuss the structural refinement of this material for improving uptakes and selectivity of gases. In the structure of the C_{60} intercalated graphite, two geometrical parameters are concerned, i.e., the interlayer distance d and the term of vdW gap g. The interlayer distance d is unchanged, because the C_{60} and the two graphite layers should remain the stable contact. As pointed out by Kuc et al., a further tuning by reducing the amount of intercalated fullerene cages is necessary to enhance H_2 loadings, which are interesting for technical applications.[16] It seems that a rational increase of g can achieve this aim. Recently, with the first-principles method, Wu and Zeng have designed a novel type material of periodic graphene nanobuds

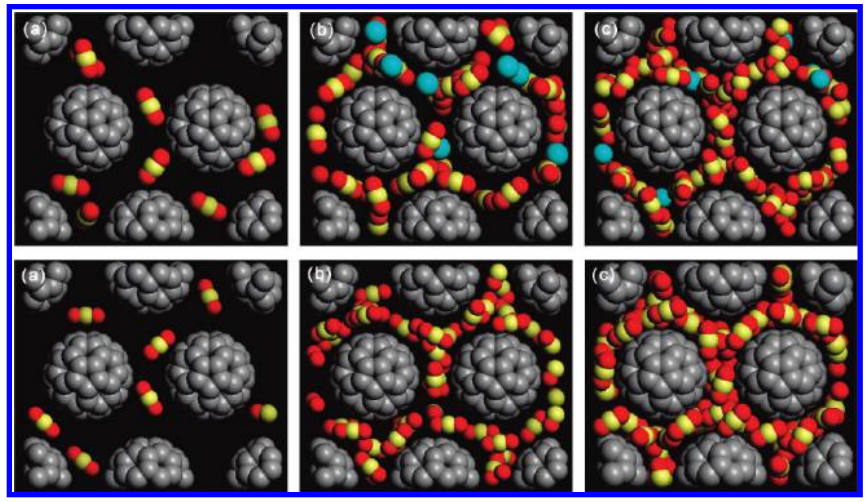

Figure 9. Snapshots of binary mixture adsorption in C_{60} intercalated graphite at 298 K and equimolar composition: top, CH_4-CO_2 mixture; bottom, N_2-CO_2 mixture; (a) 0.001 MPa; (b) 0.1 MPa; (c) 6 MPa.

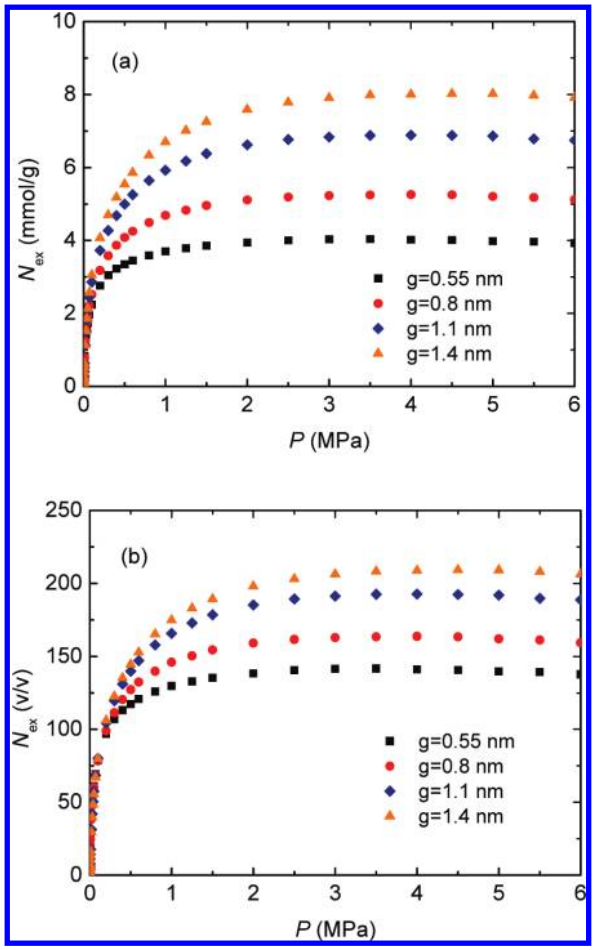

Figure 10. Excess adsorption isotherms of pure CH_4 in C_{60} intercalated graphite at 298 K and different *g*: (a) in units of mmol/g; (b) in units of v/v.

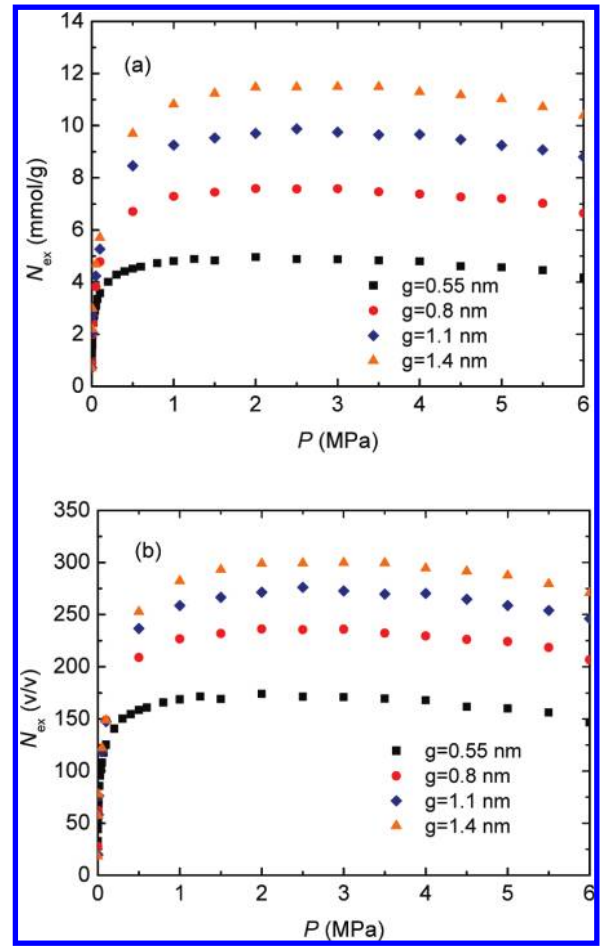

Figure 11. Excess adsorption isotherms of pure CO_2 in C_{60} intercalated graphite at 298 K and different *g*: (a) in units of mmol/g; (b) in units of v/v.

(PGNB) and found that the C_{60} fullerenes are covalently bonded to a graphene monolayer.[40] Their study provides a possibility that the distance between the C_{60} fullerenes may be controllable in synthesis or modification of the material. Consequently, we only explore the effect of parameter *g* on gas storage and purification.

Figures 10 and 11 show the excess adsorption isotherms of pure CH_4 and CO_2 at different *g*. All the isotherms reach their saturation states at the pressure range studied. Furthermore, if the parameter *g* is increased from 0.55 to 1.4 nm, the maximum uptake of CH_4 could be enhanced to 8.02 mmol/g and 209.27 v/v at 4.5 MPa, showing a rise of 98.8% for gravimetric and 47.79% for volumetric adsorption, respectively. In contrast, *g* has a more apparent influence on CO_2 storage. It corresponds to 11.50 mmol/g and 299.93 v/v at 3 MPa, raised by 122.85% and 72.33%, respectively. Actually, the improvement is mainly caused by the adjustment of material structure. As shown in Figure 12, the porosity increases monotonously with *g*, while

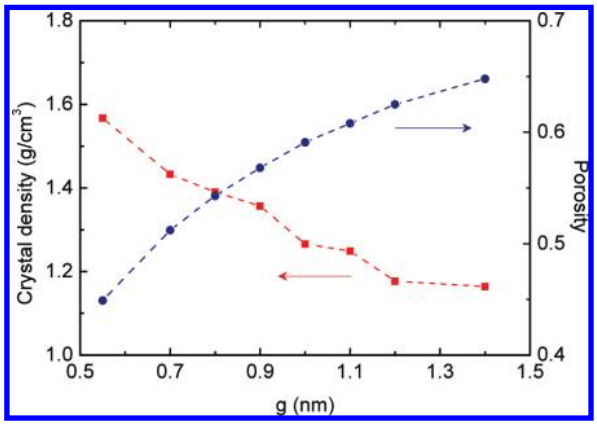

Figure 12. Crystal density and porosity of C_{60} intercalated graphite versus g. The dashed lines are to guide the eye.

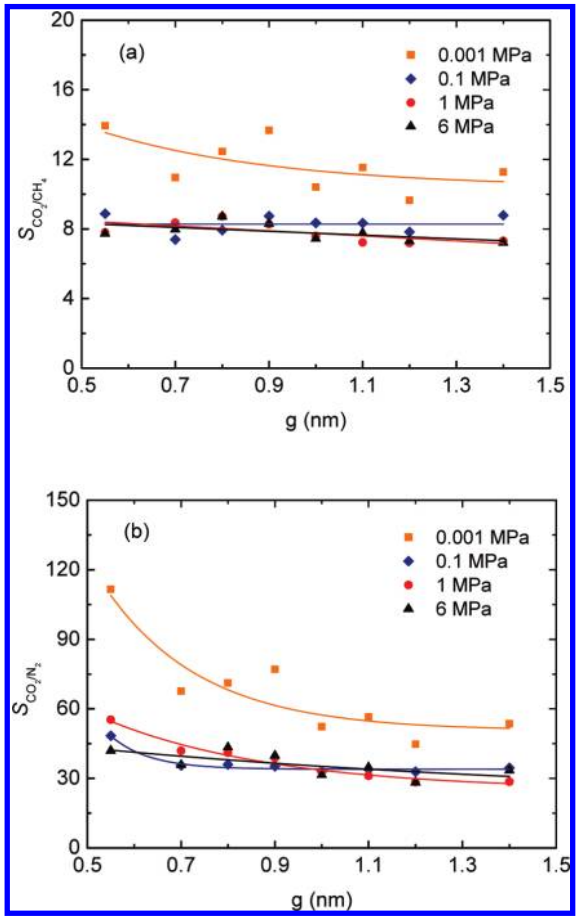

Figure 13. Adsorption selectivity of CO_2 in C_{60} intercalated graphite versus g at 298 K and equimolar composition. The lines are to guide the eye: (a) CH_4-CO_2 mixture; (b) N_2-CO_2 mixture.

the crystal density alters oppositely. A large porosity is beneficial to both gravimetric and volumetric uptakes, because more fluid molecules can be adsorbed. Similarly, the decrease of crystal density would directly induce an ascending of the gravimetric adsorption.

Figure 13 shows the dependence of adsorption selectivity of CO_2 on g at equimolar composition and different pressures. With the increase of g, the CO_2 selectivity in the N_2-CO_2 mixture decreases slowly and the downtrend becomes quick at 0.001 MPa, while it is hardly affected by the g in the CH_4-CO_2 mixture. Furthermore, the selectivity curves at $P \geq 0.1$ MPa get close each other at the whole range of g, indicating that pressure has no pronounced effect on selectivity under atmospheric conditions. The CO_2 selectivity can be at least 8 and 30 for the CH_4-CO_2 and N_2-CO_2 mixtures, respectively. In this situation, the adjacent parallel graphite layers play a more important role than C_{60} fullerenes to separate the gas mixture, because the selectivity shows a poor correlation with g. However, it is worth enlarging the g and elevating the pressure due to the fact that the CO_2 storage capacity is enhanced accordingly. From Figure 14, we see that for both mixtures, only the CO_2 uptakes at 0.001 MPa decline slightly with the increase of g. At $P \geq 0.1$ MPa, all the curves increase monotonously, where the higher the pressure, the greater the uptakes and the faster the rising trend. In particular, at 6 MPa, the uptakes of CO_2 can increase to 12 mmol/g at $g = 1.4$ nm, giving a 200% increment for both mixtures. In conclusion, the condition of $g = 1.4$ nm and 6 MPa is recommended for CO_2 purification.

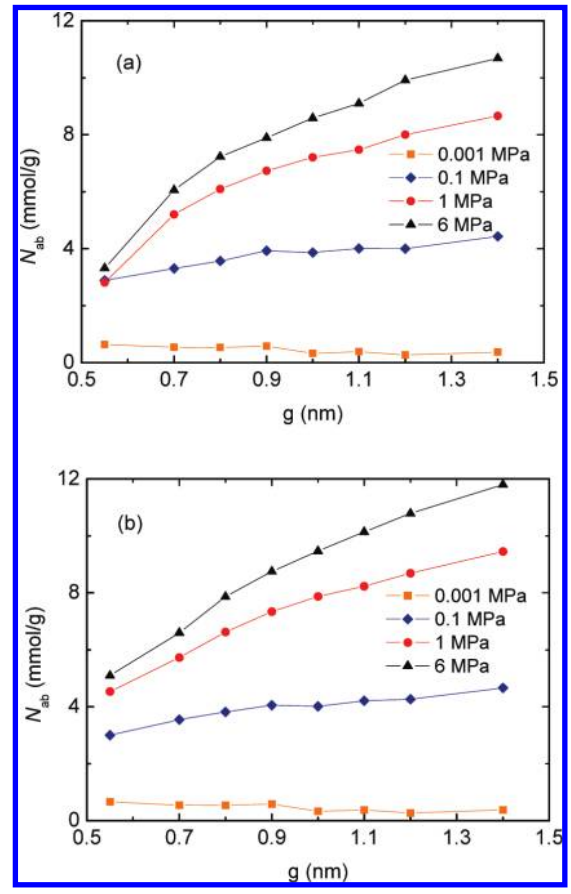

Figure 14. Absolute adsorption amount of CO_2 in C_{60} intercalated graphite versus g at 298 K and equimolar composition: (a) CH_4-CO_2 mixture; (b) N_2-CO_2 mixture. The lines are to guide the eye.

Conclusions

Gas storage and purification in the $N_2-CH_4-CO_2$ system by the C_{60} intercalated graphite were studied for the first time by using GCMC simulations and adsorption theory. In the GCMC simulation, the C_{60} intercalated graphite was constructed by tailoring 3 parallel carbon graphite layers and 16 hexagonally arranged C_{60} fullerenes into a rectangular box. The classical LJ potential was used to calculate the interactions among N_2, CH_4, and adsorbent, and the 3-site EPM2 model was adopted for CO_2 molecule.

By analyzing the adsorption isotherms, isosteric heats, and snapshots of pure gases, we found that the pristine material is not suitable for gas storage. This is because the material has a

low porosity of 0.45 and a large crystal density of 1.57 g/cm^3. Accordingly, the maximum excess uptakes only give 4.04 mmol/g for CH_4 and 4.96 mmol/g for CO_2 at room temperature. However, the Henry constant of CO_2 (0.939 mmol/kPa) shows a great advantage over other species, implying the possibility of separating CO_2 from the gas mixture with the material.

The adsorption separation was further explored for the CH_4-CO_2 and N_2-CO_2 binary systems. The DSLF equation was fitted to the GCMC simulation of pure adsorption isotherms, and they are in good agreement. With the available model parameters, the fractional uptake and selectivity were predicted by IAST and compared with the GCMC simulation. Although the IAST predicts the selectivity slightly higher than the GCMC method, their trend of the selectivity curves is basically consistent. In addition, at $P > 0.2$ MPa, the selectivity is not influenced by the bulk composition, while at $P < 0.1$ MPa, separating CO_2 via the C_{60} intercalated graphite is effective for a rich CO_2 mixture. With the increase of pressure, the selectivity of CO_2 declines gradually and stabilizes at 8 for CH_4-CO_2 and 50 for the N_2-CO_2 mixture, respectively. It suggests that the C_{60} intercalated graphite is a promising adsorbent for CO_2 purification.

To improve gas adsorption and separation, we finally tailor the structural parameter g of the C_{60} intercalated graphite. At $g = 1.4$ nm, the gravimetric uptake exhibits a rise of 98.8% and 122.85% for pure CH_4 and CO_2 adsorption, respectively. While for volumetric adsorption, it corresponds to an improvement of 47.79% and 72.33%, respectively. The improvement is mainly attributed to the decreased crystal density and the increased porosity produced by an enlargement of g. Interestingly, at $P \geq 0.1$ MPa, the adsorption selectivity of CO_2 is basically not influenced by the increase of g for the CH_4-CO_2 mixture, while it only slightly declines for the N_2-CO_2 mixture. It indicates that the parallel graphite layers play a more important role than C_{60} fullerenes in gas separation. However, it is necessary to enlarge the g, because the fractional CO_2 uptake is enhanced accordingly. At the condition of $g = 1.4$ nm and $P = 6$ MPa, the CO_2 adsorption can reach 12 mmol/g, giving a 200% increment for both mixtures.

In conclusion, this work suggests that the C_{60} intercalated graphite could be a suitable material for CO_2 purification, especially for the N_2-CO_2 system at room temperature. It is expected that our simulations will be verified experimentally in the future.

Acknowledgment

This work is supported by the NSF of China (Nos. 20806003, 20736002), the Young Scholars Fund of BUCT, the Guangzhou Center for Gas Hydrate Research, Chinese Academy of Sciences (No. CASHYD0907s3), National Science and Research Foundation (ZD0901), Huo Yingdong Fundamental Research Foundation (No. 121070), and Chemical Grid Project of BUCT.

Literature Cited

(1) Peng, X.; Cao, D. P.; Wang, W. C. Heterogeneity characterization of ordered mesoporous carbon adsorbent CMK-1 for methane and hydrogen storage: GCMC simulation and comparison with experiment. *J. Phys. Chem. C* **2008**, *112* (33), 13024–13036.

(2) Peng, X.; Cao, D. P.; Wang, W. C. Computational characterization of hexagonally ordered carbon nanopipes CMK-5 and structural optimization for H_2 storage. *Langmuir* **2009**, *25* (18), 10863–10872.

(3) Peng, X.; Wang, W. C.; Xue, R. S.; Shen, Z. M. Adsorption separation of CH_4/CO_2 on mesocarbon microbeads: experiment and modeling. *AIChE J.* **2006**, *52* (3), 994–1003.

(4) Peng, X.; Cao, D. P.; Zhao, J. S. Grand canonical Monte Carlo simulation of methane-carbon dioxide mixtures on ordered mesoporous carbon CMK-1. *Sep. Purif. Technol.* **2009**, *68* (1), 50–60.

(5) Wang, Q. Y.; Johnson, J. K. Computer simulations of hydrogen adsorption on graphite nanofibers. *J. Phys. Chem. B* **1999**, *103* (2), 277–281.

(6) Chambers, A.; Park, C.; Baker, R.; Rodriguez, N. Hydrogen storage in graphite nanofibers. *J. Phys. Chem. B* **1998**, *102* (22), 4253–4256.

(7) Park, C.; Anderson, P.; Chambers, A.; Tan, C.; Hidalgo, R.; Rodriguez, N. Further studies of hydrogen with graphite nanofibers. *J. Phys. Chem. B* **1999**, *103* (48), 10572–10581.

(8) Wang, Q. Y.; Johnson, J. K. Molecular simulation of hydrogen adsorption in single-walled carbon nanotubes and idealized carbon slit pores. *J. Chem. Phys.* **1999**, *110* (1), 577–586.

(9) Patchkovskii, S.; Tse, J. S.; Yurchenko, S. N.; Zhechkov, L.; Heine, T.; Seifert, G. Graphene nanostructures as tunable storage media for molecular hydrogen. *Proc. Natl. Acad. Sci. U.S.A.* **2005**, *102* (30), 10439–10444.

(10) Aga, R. S.; Fu, C. L.; Krčmar, M.; Morris, J. R. Theoretical investigation of the effect of graphite interlayer spacing on hydrogen absorption. *Phys. Rev. B* **2007**, *76* (16), 165404–165410.

(11) Kowalczyk, P.; Tanaka, H.; Hołyst, R.; Kaneko, K.; Ohmori, T.; Miyamoto, J. Storage of hydrogen at 303 K in graphite slitlike pores from grand canonical Monte Carlo simulation. *J. Phys. Chem. B* **2005**, *109* (36), 17174–17183.

(12) Kroto, H. W.; Heath, J. R.; O'Brien, S. C.; Curl, R. F.; Smalley, R. E. C_{60}: buckminsterfullerene. *Nature* **1985**, *318*, 162–163.

(13) Krätschmer, W.; Lamb, L. D.; Fostiropoulos, K.; Huffman, D. R. Solid C_{60}: a new form of carbon. *Nature* **1990**, *347*, 354–358.

(14) Saito, S.; Oshiyama, A. Design of C_{60}-graphite cointercalation compounds. *Phys. Rev. B* **1994**, *49* (24), 17413–17419.

(15) Gupta, V.; Scharffa, P.; Rischa, K.; Romanusb, H.; Müller, R. Synthesis of C_{60} intercalated graphite. *Solid State Commun.* **2004**, *131* (3–4), 153–155.

(16) Kuc, A.; Zhechkov, L.; Patchkovskii, S.; Seifert, G.; Heine, T. Hydrogen sieving and storage in fullerene intercalated graphite. *Nano Lett.* **2007**, *7* (1), 1–5.

(17) Benson, S. M.; Orr, J. Carbon dioxide capture and storage. *MRS Bull.* **2008**, *33*, 303–305.

(18) Olajire, A. A. CO_2 capture and separation technologies for end-of-pipe applications - A review. *Energy* **2010**, *35* (6), 2610–2628.

(19) Terzyk, A. P.; Furmaniak, S.; Gauden, P. A.; Kowalczyk, P. Fullerene-intercalated graphene nano-containers — mechanism of argon adsorption and high-pressure CH_4 and CO_2 storage capacities. *Ads. Sci. Technol.* **2009**, *27* (3), 281–296.

(20) Pikunic, J.; Clinard, C.; Cohaut, N.; Gubbins, K. E.; Guet, J.; Pellenq, R.; Rannou, I.; Rouzaud, J. Structural modeling of porous carbons: constrained reverse Monte Carlo method. *Langmuir* **2003**, *19* (20), 8565–8582.

(21) Ohkubo, T.; Miyawaki, J.; Kaneko, K.; Ryoo, R.; Seaton, N. A. Adsorption properties of templated mesoporous carbon (CMK-1) for nitrogen and supercritical methanes—experiment and GCMC simulation. *J. Phys. Chem. B* **2002**, *106* (25), 6523–6528.

(22) Harris, J. G.; Yung, K. H. Carbon dioxide liquid-vapor coexistence curve and critical properties as predicted by a simple molecular model. *J. Phys. Chem.* **1995**, *99* (31), 12021–12024.

(23) Peng, X.; Zhao, J. S.; Cao, D. P. Adsorption of carbon dioxide of 1-site and 3-site models in pillared clays: a Gibbs ensemble Monte Carlo simulation. *J. Colloid Interface Sci.* **2007**, *310* (2), 391–401.

(24) Frenkel, D.; Smit, B. *Understanding molecular simulations*; Academic Press: New York, 2002.

(25) Allen, M. P.; Tildesley, D. J. *Computer simulation of liquids*; Clarendon Press: Oxford, 1987.

(26) Peng, D. Y.; Robinson, D. B. A new two-constant equation of state. *Ind Eng Chem Fundam.* **1976**, *15* (1), 59–64.

(27) Reid, R. C.; Prausnitz, J. M.; Poling, B. E. *The properties of gases and liquids*; McGraw-Hill Press: New York, 1987.

(28) Gupta, A.; Chempath, S.; Sanborn, M. J.; Clark, L. A.; Snurr, R. Q. Object-Oriented Programming Paradigms for Molecular Modeling. *Mol. Simul.* **2003**, *29* (1), 29–46.

(29) Thomson, K. T.; Gubbins, K. E. Modeling structural morphology of microporous carbons by reverse Monte Carlo. *Langmuir* **2000**, *16* (13), 5761–73.

(30) Garberoglio, G. Computer simulation of the adsorption of light gases in covalent organic frameworks. *Langmuir* **2007**, *23* (24), 12154–12158.

(31) Babarao, R.; Hu, Z. Q.; Jiang, J. W.; Chempath, S.; Sandler, S. I. Storage and separation of CO_2 and CH_4 in silicalite, C_{168} schwarzite, and

IRMOF-1: a comparative study from Monte Carlo simulation. *Langmuir* **2007**, *23* (2), 659–666.

(32) Myers, A. L.; Prausnitz, J. M. Thermodynamics of mixed-gas adsorption. *AIChE J.* **1965**, *11* (1), 121–127.

(33) Sudibandriyo, M.; Pan, Z. J.; Fitzgerald, J. E.; Robinson, R. L., Jr.; Gasem, K. A. M. Adsorption of methane, nitrogen, carbon dioxide, and their binary mixtures on dry activated carbon at 318.2 K and pressures up to 13.6 MPa. *Langmuir* **2003**, *19* (13), 5323–5331.

(34) Ma, S.; Sun, D.; Simmons, J. M.; Collier, C. D.; Yuan, D.; Zhou, H. C. Metal-organic framework from an anthracene derivative containing nanoscopic cages exhibiting high methane uptake. *J. Am. Chem. Soc.* **2008**, *130* (3), 1012–1016.

(35) Kurniawan, Y.; Bhatia, S. K.; Rudolph, V. Simulation of binary mixture adsorption of methane and CO_2 at supercritical conditions in carbons. *AIChE J.* **2006**, *52* (3), 957–967.

(36) Huang, L. L.; Zhang, L. Z.; Shao, Q.; Lu, L. H.; Lu, X. H.; Jiang, S. Y.; Shen, W. F. Simulations of binary mixture adsorption of carbon dioxide and methane in carbon nanotubes: temperature, pressure, and pore size effects. *J. Phys. Chem. C* **2007**, *111* (32), 11912–11920.

(37) Jiang, J. W.; Sandler, S. I. Separation of CO_2 and N_2 by adsorption in C_{168} schwarzite: a combination of quantum mechanics and molecular simulation study. *J. Am. Chem. Soc.* **2005**, *127* (34), 11989–11997.

(38) Bojan, M. J.; Steele, W. A. Virial coefficients for N_2 and CO adsorbed on the graphite basal plane. *Langmuir* **1987**, *3* (1), 116–120.

(39) Bojan, M. J.; Steele, W. A. Interactions of diatomic molecules with graphite. *Langmuir* **1987**, *3* (6), 1123–1127.

(40) Wu, X. J.; Zeng, X. C. Periodic graphene nanobuds. *Nano Lett.* **2009**, *9* (1), 250–256.

Received for review May 7, 2010
Revised manuscript received July 25, 2010
Accepted July 26, 2010

IE1010433